

Tunable ferroelectricity in hBN intercalated twisted double-layer graphene

Yibo Wang^{1,*}, Siqu Jiang^{1,+}, Jingkuan Xiao¹, Xiaofan Cai¹, Di Zhang¹, Ping Wang¹, Guodong Ma¹, Yaqing Han¹, Jiabei Huang¹, Kenji Watanabe², Takashi Taniguchi², Alexander S. Mayorov^{1,*}, and Geliang Yu^{1,3,*}

¹National Laboratory of Solid State Microstructures and School of Physics, Nanjing University, Nanjing 210093, People's Republic of China.

²National Institute for Materials Science, 1-1 Namiki, Tsukuba 305-0044 Japan.

³Collaborative Innovation Centre of Advanced Microstructures, Nanjing University, Nanjing 210093, People's Republic of China.

*yibowang@nju.edu.cn, mayorov@nju.edu.cn, yugeliang@nju.edu.cn

+These authors contributed equally to this work.

ABSTRACT

Van der Waals (vdW) assembly of two-dimensional materials has been long recognized as a powerful tool to create unique systems with properties that cannot be found in natural compounds¹. However, among the variety of vdW heterostructures and their various properties, only a few have revealed metallic and ferroelectric behaviour signatures^{2,3}. Here we show ferroelectric semimetal made of double-gated double-layer graphene separated by an atomically thin crystal of hexagonal boron nitride, which demonstrating high room temperature mobility of the order of $10 \text{ m}^2\text{V}^{-1}\text{s}^{-1}$ and exhibits robust ambipolar switching in response to the external electric field. The observed hysteresis is tunable, reversible and persists above room temperature. Our fabrication method expands the family of ferroelectric vdW compounds and offers a route for developing novel phase-changing devices.

Introduction

Competing phases in condensed matter demonstrate the variety of physics phenomena: superconductivity and ferromagnetism, charge density wave and superconductivity⁴ to name a few. The recently investigated ferroelectric semimetal such as WTe_2 ^{2,3} as an example of an unintuitive interplay between polarization and free charge, which seems at first glance, should screen the former. Generally, metallic properties of a material do not favour macroscopic polarization, which means that ferroelectricity as a phenomenon is observed in many ferroelectrics of dielectric nature or semiconducting materials. Only a few examples exist for metallic ferroelectrics and even less number of candidates to show hysteretic behaviour⁵. However, there is one experimental evidence of natural 2D ferroelectric semimetal at room temperature: a few-layer WTe_2 ³ made by exfoliation, and another example is artificially made 2D polar metal based on superlattices $\text{BaTiO}_3/\text{SrTiO}_3/\text{LaTiO}_3$ using advantage of molecular beam epitaxy growth⁶. Both of these materials demonstrate a room-temperature ferroelectric effect. A ferroelectric structural transition occurs in bulk (3D) LiOsO_3 crystals at 140K⁷. The interest in these materials is hidden in the possibility of creating new quantum states, including coexisting ferroelectric, ferromagnetic, and superconducting phases⁷, use them for functional nanoelectronics applications². It is relevant to the combination of memory effects and conduction modulation, which improves transistor performance^{8,9}.

Graphene has high-mobility charge carriers at room temperature with acoustic phonon scattering as a limiting factor¹⁰. Bilayer graphene demonstrates lower mobility at room temperature than monolayer graphene, but it is still much larger than any other semiconductors, and semimetals known^{11,12,13}. Therefore, it could improve the transport properties of ferroelectric metals based on vdW graphene heterostructures. Previously a breakthrough idea of changing properties of two-dimensional materials by staking them in a different order is useful for constructing the new artificially made vdW heterostructures¹. For a ferroelectric metal to exist, several criteria need to be: second-order phase transition, breaking inversion symmetry, polarization switchability⁵.

Here we explore this general idea to create a recently discovered class of materials that combine semimetallic and ferroelectric properties in a single material¹⁴. The effect of the moiré pattern reveals the possibility of forming a strong ferroelectric characteristic for conventional 2D materials such as hexagonal boron nitride(hBN) and bilayer graphene¹⁵. Breaking of the inversion symmetry occurs by mechanical stacking of two individual layers under small angle rotation, which

opens a new path to create different physical effects in graphene, besides the well know proximity of graphene to ferromagnets, superconductors, 2D materials with spin-orbit interactions. Here we study electronic properties and reproduce the ferroelectric effect in bilayer graphene intercalated with a monolayer hBN up to 325K and demonstrate a metal-to-insulator transition ferroelectric effect in graphene.

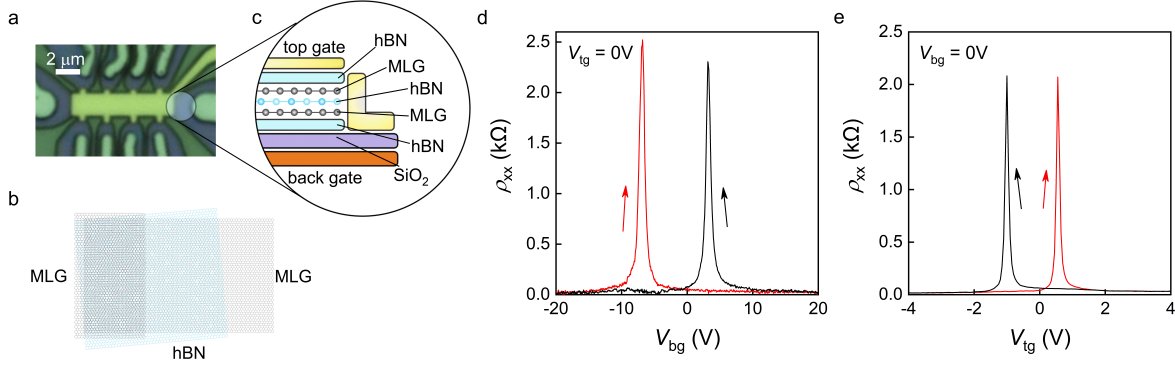


Figure 1. Hexagonal boron nitride-separated quasi-twisted bilayer graphene. **a.** Optical photograph of our Hall bar device. An encapsulated qTBG heterostructure is connected to metal leads (dull green) and endowed with gold top gate(bright green) and bottom silicon gate electrodes. **b.** Schematic of the triple-layer structure. Two MLG layers are twisted by a small twist angle. **c.** The schematic of the qTBG device with top and bottom gates. **d** and **e.** The device's resistivity measured as a function of V_{bg} and V_{tg} at 2.1K for $V_{tg} = 0V$ and $V_{bg} = 0V$, respectively.

Fabrication

Our device is a multiterminal Hall bar (Fig. 1a) made of quasi-twisted bilayer graphene (qTBG) using standard dry transfer technique¹⁶. Graphene layers in such qTBG are separated by a monolayer of hexagonal boron nitride, allowing the graphene layers to be tunnelled transparent. The sandwich is encapsulated between two relatively thick hexagonal boron nitride slabs protecting graphene layers from the environment (Fig. 1b). The qTBG heterostructure is connected to metal contacts¹⁰ and endowed with top and bottom gate electrodes allowing independent control over the carrier density in each layer (n_t and n_b , respectively) and relative displacement field between the layers.

Results

Electrical transport measurements are carried out in a ^3He variable temperature inset system using the standard low-frequency lock-in technique. Fig. 1c shows our qTBG sample's resistivity as a function of back-gate voltage, V_{bg} , measured at $T = 2.1\text{K}$ and zero top gate voltage, $V_{tg} = 0V$. It exhibits familiar for high-mobility bilayer graphene behaviour with a sharp peak of about $2\text{k}\Omega$ corresponding to the charge neutrality point (CNP), followed by a rapid decrease with increasing V_{bg} . When the gate voltage's sweep direction is reversed, the resistivity curve is shifted so that the CNP appears at 7V , more than 10V away from its initial position. The observed hysteresis is robust and reproduces itself for numerous gate (top and bottom) voltage sweep loops without an apparent sign of degradation of the hysteretic behaviour. A similar hysteresis is observed for the top gate sweep measured at $V_{bg} = 0V$. Notice the CNP position, which is shifted to positive top gate voltages for the forward sweep and negative voltage for the backward sweep.

We review observed hysteretic behaviour of resistivity of the qTBG intercalated with monolayer hBN, in more details. Previously, a moiré heterostructure hBN/bilayer graphene/hBN has demonstrated a similar hysteresis at low temperatures¹⁵. The resistivity map is measured as a function of the back gate voltage which charges from $-40V$ to $40V$ for the forward sweep Fig. 2a and $40V$ to $-40V$ for the backward sweep (Fig. 2b). Both maps are measured at 2.1K , and during the sweep, the top gate voltage is fixed. The top gate voltage changes from negative to positive values (from $-5V$ to $4V$). The dark region shows a noticeable difference in the resistivity peak position between the forward and backward sweeps. We plot Fig. 2c the maximum resistivity for the forward and backward back gate voltage sweeps to characterize the hysteresis. The hysteretic behaviour illustrates internal polarization in the heterostructure¹⁵, which changes the charge carrier concentration in both graphene layers. The external electric field created by the back and top gate voltages can reverse this polarization by applying a large back gate voltage ($|V_{bg}| > 10V$) or top gate voltage $V_{tg} < -2.2V$ and $V_{tg} > 1.5V$. The peak shifts linearly in the range of V_{bg} from $-9.1V$

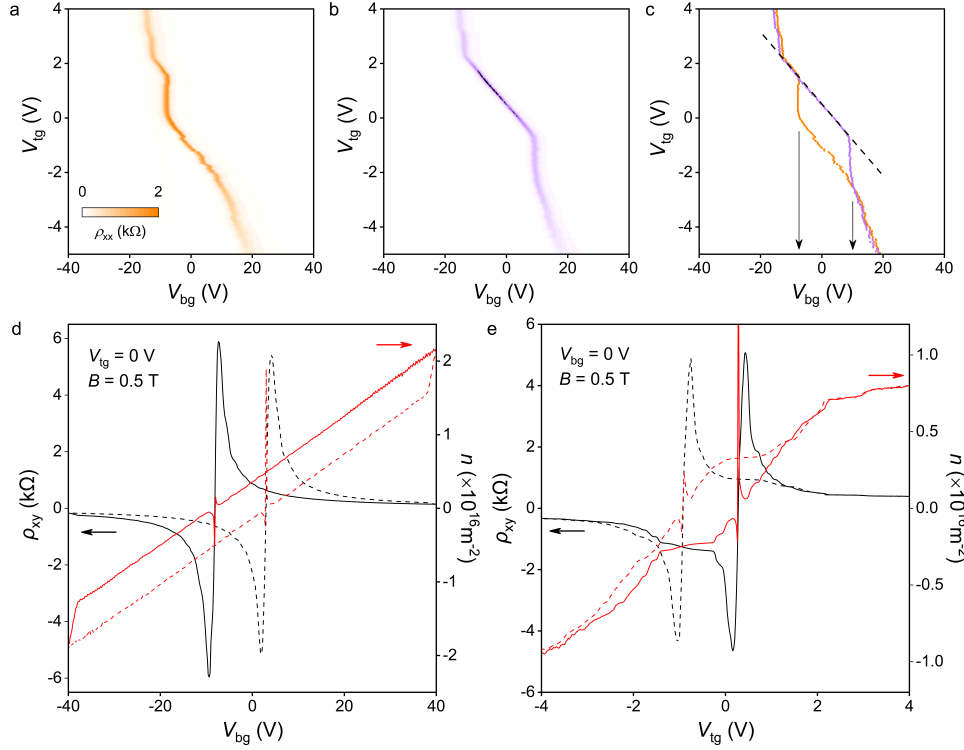


Figure 2. Ferroelectric hysteresis at 2.1K. **a-b** The sample's resistivity as a function of the back gate and top gate voltages for the forward **a** and backward **b** back gate voltage sweeps at fixed V_{tg} . **c**. The maximum of the resistivity for the forward and backward as a function of the top gate and back gate voltages. The dashed line is the best fit for the forward and backward sweep's resistivity maxima in the linear ferroelectric regime. **d**. Hall effect measured at $B = 0.5\text{ T}$ for forward (solid black curve) and backward (dashed black curve) sweeps as a function of back gate voltage at $V_{tg} = 0\text{ V}$. The red curves show corresponding concentrations calculated from the Hall voltage. **e**. Hall effect measured at $B = 0.5\text{ T}$ for the forward (solid black curve) and backward (dashed black curve) sweeps as a function of top gate voltage at $V_{bg} = 0\text{ V}$. The red curves show corresponding concentrations calculated from the Hall voltage.

to 9.7V, which corresponds to a linear polarization for ferroelectrics¹⁷. The top gate's efficiency with respect to the bottom gate cannot be determined from the top and bottom hBN thicknesses (42.6nm and 111nm, respectively) using a small dielectric constant for hBN. If the relative dielectric constant for hBN is taken as 5, then the expected efficiency is about 11.6. However, the dashed lines in Fig.2c correspond to the ratio of $V_{bg}/V_{tg} = 7.6 \pm 0.1$. Therefore, the dielectric environment of graphene is significantly distorted by the ferroelectric effect. In the regions without hysteresis, the resistivity peak shift also does not correspond to the gate's efficiency. It enters the nonlinear polarization regime of ferroelectric, which is commonly attributed to the paraelectric phase¹⁷. In the paraelectric phase, the dielectric constant is not linear, and the resistivity of the structure depends strongly on the properties of hBN layers. To the best of our knowledge, this observation has not been reported before in 2D heterostructures.

The average concentration in the system then can be determined by the Hall effect (see supplementary). Calculations of the Hall concentration as a function of back-gate voltage at $V_{tg} = 0\text{ V}$ are shown in Fig.2d, e. The position of the maximum is shifted between the forward and backward shift on the same amount when the efficiency of the top gate is taken into account. We notice here that the view of this hysteresis and the positions of maxima and minima do not change if top gate voltage sweeps are used at fixed V_{bg} (See supplementary).

Finally, we characterized the temperature dependence of the resistivity for the forward and backward sweeps. The peak resistivity is reducing with increasing temperature as expected for both monolayer and bilayer graphene, and the separation between peaks, which is related to spontaneous polarization in our structure, is decreasing with increasing temperature. Still, it does not disappear entirely, even at the maximum available temperature of 325K (Fig.3b). The full data set is shown in the

supplementary. The cross-over density between metallic ($d\rho/dT < 0$) and insulator ($d\rho/dT > 0$) states is equal to $5 \times 10^{10} \text{ cm}^{-2}$, which is in agreement with previous report¹⁸. The corresponding mobility is found to be better than $10 \text{ m}^2 \text{ V}^{-1} \text{ s}^{-1}$ at room temperature (Fig.3d), which is higher than in bilayer graphene¹⁹ and comparable with acoustic phonon limited mobility in monolayer graphene¹⁰. The charge carrier mobility reduces with increasing temperature, as shown in Fig.3d linearly.

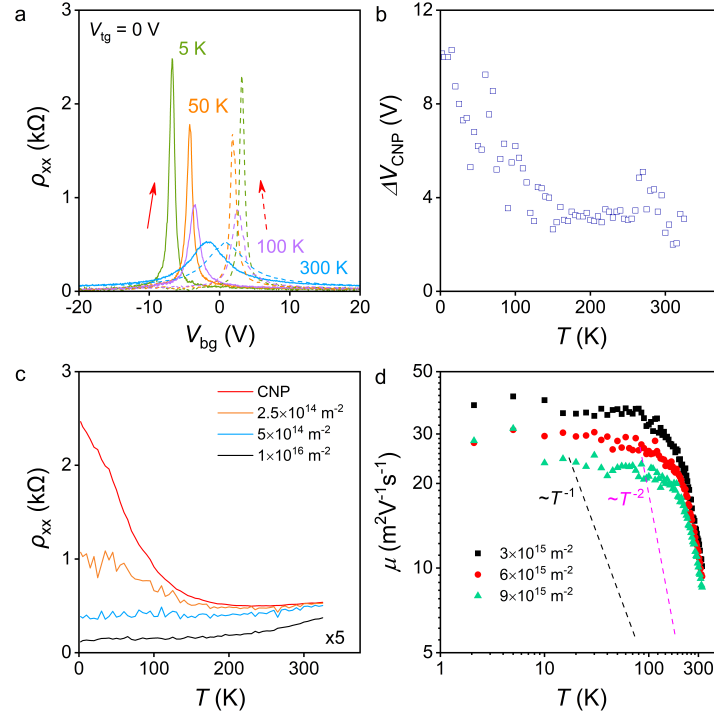


Figure 3. Transport properties at high temperatures. **a.** Temperature dependence of the resistivity as a function of back gate voltage at $V_{tg} = 0$ V for the forward (solid style) and backward sweeps (dashed style) for four selected temperatures. **b.** The voltage difference between CNP positions of the backward and forward sweeps. The temperature changes from 2 K to 325 K. **c.** The temperature dependence of the resistivity for the forward sweeps for different electron concentrations. The smallest resistivity is multiplied by 5. **d.** The mobility of electron gas as a function of temperature measured at $3 \times 10^{15} \text{ m}^{-2}$, $6 \times 10^{15} \text{ m}^{-2}$ and $9 \times 10^{15} \text{ m}^{-2}$. The dashed lines are guides for eyes.

Discussion

Previously a strong ferroelectric effect was observed in aligned and rotated by 30° hBN/bilayer graphene heterostructures¹⁵. The authors argued that the different parts of a supercell could induce spontaneous polarization in such a structure. Here we study a similar system without intentional alignment between hBN and graphene layers. The absence of any supercell at low energy could be justified by the gate voltage dependence of the resistance. In this case, the band structure should have more features at low energy, which creates extra CNPs as was reported in²⁰. Also, Brown-Zak oscillations²¹, which could be an indication of alignment between graphene and hBN, are not observed in our device. Therefore, our system's ferroelectric effect could not be of the same origin as in the intentionally aligned graphene/hBN structure¹⁵. However, we could not exclude 30° rotation¹⁵ or the inversion symmetry breaking in the vertical graphene/hBN/graphene heterostructure as a cause of ferroelectricity. The twisted hBN layers can demonstrate the ferroelectric effect²². This observation was reported in^{23, 24}. If we assume that the monolayer hBN can be easily twisted when placed between two graphene layers. In that case, the polarization can be created by the top hBN and monolayer hBN or between monolayer hBN and bottom hBN layers. This effect needs further investigation.

Mobility of the charge carriers in graphene at high temperature is limited by acoustic phonon scattering¹⁰. The temperature dependence of mobility is inversely proportional to temperature. This observation is valid for graphene and its bilayer²⁵. The temperature dependence of resistivity is proportional to $\rho \propto T$ in the case of twisted bilayer graphene, which was observed experimentally²⁶ and predicted theoretically²⁷ for small angles of rotation. Our observations demonstrate inverse parabolic

dependence of the mobility $\rho \propto T^{-2}$ as shown in Fig.3d, which we attribute to the contribution of optical phonons in hBN substrate²⁸ or polar optical phonons²⁹ in agreement with ferroelectric nature of our structure. The low-temperature mobility is limited by scattering at the edges of the sample.

Methods

0.1 Transport measurements

The device was measured in an Oxford Instruments TeslatronPT cryogen-free superconducting magnet system equipped with Oxford Instruments HelioxVT Sorption Pumped ³He Refrigerator insert (300mK,14T) and the magnetic field applied perpendicular to the plane of the film. Stanford Research Systems SR830 lock-in is used to apply a AC bias current with a 100MOhm bias resistor at a frequency of 13.333 Hz, and Keithley 2614B SourceMeters were used to apply DC current with a 100MOhm bias resistor. Keithley 2400 SourceMeters were used to apply voltages to the gates.

0.2 AFM and Raman measurements

AFM measurements are performed with a Bruker Dimension Fastscan system at tapping mode. Scan area of the bottom/top hBN are shown in the right/left red dotted boxes in the supplementary. The length to width ratio is 1.16. The width of the sample is 2.7 μ m. The top and bottom hBN thicknesses are equal to 42.6nm and 111nm, respectively.

Room temperature Raman scattering is performed using a WITec/alpha 300R confocal microscope with a 532nm laser under ambient conditions. The laser power was kept below 1mW to avoid damage or heating. The G and 2D peaks in the Raman spectra are fitted with Lorentzian. Typical Raman spectra of different positions of the heterostructure are plotted in the Supplementary.

References

1. Geim, A. K. & Grigorieva, I. V. Van der waals heterostructures. *Nature* **499**, 419–425, DOI: <https://www.nature.com/articles/nature12385> (2013).
2. Sharma, P. *et al.* A room-temperature ferroelectric semimetal. *Sci. Adv.* **5**, eaax5080, DOI: <https://advances.sciencemag.org/content/5/7/eaax5080> (2019).
3. Fei, Z. *et al.* Ferroelectric switching of a two-dimensional metal. *Nature* **560**, 336–339, DOI: <https://doi.org/10.1038/s41586-018-0336-3> (2018).
4. Xi, X. *et al.* Strongly enhanced charge-density-wave order in monolayer nbse₂. *Nat. Nanotech.* **10**, 765–769, DOI: <https://doi.org/10.1038/nnano.2015.143> (2015).
5. Zhou, W. X. & Ariando, A. Review on ferroelectric/polar metals. *Jpn. J. Appl. Phys.* **59**, SI0802, DOI: <https://doi.org/10.35848/1347-4065/ab8bbf> (2020).
6. Cao, Y. *et al.* Artificial two-dimensional polar metal at room temperature. *Nat. Commun.* **9**, 1547, DOI: [10.1038/s41467-018-03964-9](https://doi.org/10.1038/s41467-018-03964-9) (2018).
7. Shi, Y. *et al.* A ferroelectric-like structural transition in a metal. *Nat. Mater.* **12**, 1024–1027, DOI: <https://doi.org/10.1038/nmat3754> (2013).
8. Liu, X. *et al.* Vertical ferroelectric switching by in-plane sliding of two-dimensional bilayer wte₂. *Nanoscale* **11**, 18575–18581, DOI: <https://doi.org/10.1039/C9NR05404A> (2019).
9. Si, M. *et al.* A ferroelectric semiconductor field-effect transistor. *Nat. Nanoelectron.* **2**, 580–586, DOI: <https://doi.org/10.1038/s41928-019-0338-7> (2019).
10. Wang, L. *et al.* One-dimensional electrical contact to a two-dimensional material. *Science* **342**, 614–617, DOI: <https://doi.org/10.1126/science.1244358> (2013).
11. Dean, C. R. *et al.* Boron nitride substrates for high-quality graphene electronics. *Nat. Nanotechnol.* **5**, 722–726, DOI: <https://doi.org/10.1038/nnano.2010.172> (2010).
12. Mayorov, A. S. *et al.* Micrometer-scale ballistic transport in encapsulated graphene at room temperature. *Nano Lett.* **11**, 2396–2399, DOI: <https://doi.org/10.1021/nl200758b> (2011).
13. Castro Neto, A. H., Guinea, F., Peres, N. M. R., Novoselov, K. S. & Geim, A. K. The electronic properties of graphene. *Rev. Mod. Phys.* **81**, 109–162, DOI: <https://link.aps.org/doi/10.1103/RevModPhys.81.109> (2009).

14. Puggioni, D., Giovannetti, G., Capone, M. & Rondinelli, J. M. Design of a mott multiferroic from a nonmagnetic polar metal. *Phys. Rev. Lett.* **115**, 087202, DOI: <https://link.aps.org/doi/10.1103/PhysRevLett.115.087202> (2015).
15. Zheng, Z. *et al.* Unconventional ferroelectricity in moiré heterostructures. *Nature* **588**, 71–76, DOI: <https://doi.org/10.1038/s41586-020-2970-9> (2020).
16. Kretinin, A. V. *et al.* Electronic properties of graphene encapsulated with different two-dimensional atomic crystals. *Nano Lett.* **14**, 3270–3276, DOI: <https://doi.org/10.1021/nl5006542> (2014).
17. Lines, M. *Principles and applications of ferroelectrics and related materials* (Clarendon Press, Oxford England, 1977).
18. Ponomarenko, L. A. *et al.* Tunable metal–insulator transition in double-layer graphene heterostructures. *Nat. Phys.* **7**, 958–961, DOI: <https://doi.org/10.1038/nphys2114> (2011).
19. Schmitz, M. *et al.* High mobility dry-transferred cvd bilayer graphene. *Appl. Phys. Lett.* **110**, 263110, DOI: <https://doi.org/10.1063/1.4990390> (2017).
20. Wang, Z. *et al.* Composite super-moiré lattices in double-aligned graphene heterostructures. *Sci. Adv.* **5**, eaay8897, DOI: <https://doi.org/10.1126/sciadv.aay8897> (2019).
21. Kumar, R. K. *et al.* High-temperature quantum oscillations caused by recurring bloch states in graphene superlattices. *Science* **357**, 181–184, DOI: <https://doi.org/10.1126/science.aal3357> (2017).
22. Woods, C. R. *et al.* Charge-polarized interfacial superlattices in marginally twisted hexagonal boron nitride. *Nat. Commun.* **12**, 347, DOI: <https://doi.org/10.1038/s41467-020-20667-2> (2021).
23. Stern, M. V. *et al.* Interfacial ferroelectricity by van der waals sliding. *arXiv:2010.05182* (2020).
24. Yasuda, K., Wang, X., Watanabe, K., Taniguchi, T. & Jarillo-Herrero, P. Stacking-engineered ferroelectricity in bilayer boron nitride. *arXiv:2010.06600* (2020).
25. Min, H., Hwang, E. H. & Das Sarma, S. Chirality-dependent phonon-limited resistivity in multiple layers of graphene. *Phys. Rev. B* **83**, 161404, DOI: <https://link.aps.org/doi/10.1103/PhysRevB.83.161404> (2011).
26. Polshyn, H. *et al.* Large linear-in-temperature resistivity in twisted bilayer graphene. *Nat. Phys.* **15**, 1011–1016, DOI: <https://doi.org/10.1038/s41567-019-0596-3> (2019).
27. Wu, F., Hwang, E. & Das Sarma, S. Phonon-induced giant linear-in- t resistivity in magic angle twisted bilayer graphene: Ordinary strangeness and exotic superconductivity. *Phys. Rev. B* **99**, 165112, DOI: <https://link.aps.org/doi/10.1103/PhysRevB.99.165112> (2019).
28. Lin, I.-T. & Liu, J.-M. Surface polar optical phonon scattering of carriers in graphene on various substrates. *Appl. Phys. Lett.* **103**, 081606, DOI: <https://doi.org/10.1063/1.4819395> (2013).
29. Li, X., Barry, E. A., Zavada, v., Nardelli, M. B. & Kim, K. W. Surface polar phonon dominated electron transport in graphene. *Appl. Phys. Lett.* **97**, 232105, DOI: <https://doi.org/10.1063/1.3525606> (2010).

Acknowledgements

We thank B.G. Wang, K.S. Novoselov for useful discussions. This work is supported by the National Key R&D Program of China (grant nos. SQ2018YFA030066, SQ2018YFA030143), the National Natural Science Foundation of China (no. 11974169) and the Fundamental Research Funds for the Central Universities (nos. 020414380087, 020414913201), and the Basic Research Program of Jiangsu Province (Grant No. BK20190283).

Author contributions statement

A.S.M. and G.Y. designed the project. Y.W. and fabricated the samples, S.J. and J.X. performed transport measurements, X.C. and G.M. did the AFM and Raman research, K.W. and T.T. provided hBN crystals. S. J., J.X., Y.W., and A.S.M performed data analysis, D.Z., P.W., G.M., Y.H, J.H., and A.S.M provided the experimental support. Y.W., A.S.M and G.Y. wrote the manuscript. All authors participated in the discussions.

Competing interests

The authors declare no competing interests.

Additional information

Supplementary information is available for this paper at <>.

Correspondence and requests for materials should be addressed to Y.W, A.S.M. or G.Y.